Published online: 2020-01-30

Solid-State Fluorescence Enhancement of Bromine-Substituted *Trans*-Enaminone Derivatives

Hua Li[a,b]
Haiyang Shu[a,b]
Xin Wang[a,b]
Xiaofu Wu[a]
Hongkun Tian[a,b]
Hui Tong*[a,b]
Lixiang Wang*[a,b]

[a] State Key Laboratory of Polymer Physics and Chemistry, Changchun Institute of Applied Chemistry, Chinese Academy of Sciences, Changchun 130022, China
[b] University of Science and Technology of China, Hefei 230026, China
chemtonghui@ciac.ac.cn; lixiang@ciac.ac.cn.

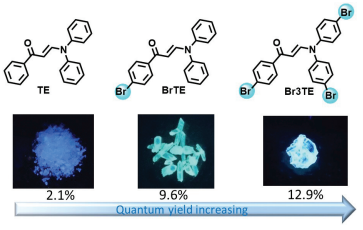

Received: 29.09.2019
Accepted after revision: 02.12.2019

DOI: 10.1055/s-0040-1701249; Art ID: om-19-0013-oa

Abstract Halogen bonding, as a kind of intermolecular interaction, has rarely been used to tune solid-state emission properties of luminescent materials, especially fluorescent materials. Herein, three *trans*-enaminone (TE) derivatives (nonbrominated TE, monobrominated BrTE, and tribrominated Br3TE) with aggregation-induced emission property have been designed and synthesized. Two types of BrTE crystals (BrTE-B and BrTE-G) with different fluorescence properties were obtained. It was observed that their solid-state fluorescence has been enhanced by the formation of halogen bonding. In particular, the crystal BrTE-G containing Br…π interactions exhibits a fluorescence quantum yield (9.6%) nearly sevenfold higher than BrTE-B, the crystal without halogen bonding (1.4%), and fivefold higher than the nonbrominated TE derivative (2.1%). By careful inspection of the single-crystal data and theoretical calculations, the high fluorescence quantum yield of BrTE-G appears to be due to halogen-bonding interactions as well as multiple stronger intermolecular interactions which may restrain molecular motions, leading to the reduced nonradiative decay rate and the enhanced radiative decay rate. Additionally, increasing the number of bromine substituents may further promote the radiative decay rate, explaining therefore the higher fluorescence quantum yield (12.5%) of Br3TE.

Key words halogen bonding, solid-state emission, aggregation-induced emission, fluorescence, crystals, enaminones

Introduction

Research studies on organic fluorophores with high emission in the solid state are appealing due to the potential applications of those molecules in organic electronics and biosensors.[1] Notoriously, the emissions of most organic fluorophores are quenched in the solid state and this seriously limits their applications.[2] To avoid the aggregation-caused quenching, a large number of conjugated or nonconjugated molecules with aggregation-induced emission (AIE) property have been studied since the first AIE molecule was proposed by Tang et al in 2001.[3] Considering the restriction of the intramolecular motion mechanism of the AIE materials, the molecular packing mode can exert an important influence on their emissive properties.[4] This may be tuned by weak interactions, such as hydrogen bonding,[5] π–π interaction,[6] and van der Waals interaction.[7] Investigating the packing modes and intermolecular interactions in crystal structures is therefore of great interest to help designing highly luminescent molecules in solid states.[8]

Halogen bonding is a strong and directional interaction between a polarized halogen atom and a Lewis base as officially defined by IUPAC in 2013.[9] This noncovalent interaction is similar to hydrogen bonding[10] and in recent years, due to its higher directionality and broader tunability, it has been established as a powerful interaction to use for self-assembly in condensed phases and for application in biological systems.[11] Halogen-bonding interactions have shown superior anion affinities and contrasting selectivities in the anion recognition and sensing process due to their electron-deficient and hydrophobic nature.[12] Furthermore, investigations on the application of halogen bonding donor systems as catalysts in organic synthesis have been also highlighted.[13] Although the importance of halogen bonding has been recognized in numerous applications, the use of halogen bonding to tune luminescence properties in the field of organic luminogens has long been overlooked.

In recent years, halogen atoms (Br, I) have been used to design highly efficient room-temperature phosphorescent materials due to their heavy atom effect which strengthens the efficiency of the intersystem crossing process between the singlet and triplet states.[14] Moreover, the formation of

halogen bonding in solid states induced the rigidification effect, which can reduce vibrational relaxations of triplets, resulting in strong phosphorescence emission.[15] Halogen bonding is also an effective strategy for tuning the solid-state fluorescence properties such as emission color, lifetime, and fluorescence intensity.[16] In a recent work, we have reported a planar bromine-substituted *cis*-enaminone fluorophore with AIE property.[17] Compared with its analogue without bromine, it exhibits a much stronger solid-state fluorescence emission because the formation of intermolecular Br…Br halogen bonding suppresses molecular motions more efficiently.

To further study the effect of halogen bonding on fluorescence enhancement, in this work we designed and synthesized three bromine-substituted *trans*-enaminone derivatives: (*E*)-3-(diphenylamino)-1-phenylprop-2-en-1-one (**TE**), (*E*)-1-(4-bromophenyl)-3-(diphenylamino)prop-2-en-1-one (**BrTE**), and (*E*)-3-(bis(4-bromophenyl)amino)-1-(4-bromophenyl)prop-2-en-1-one (**Br3TE**) (Figure 1). All the three *trans*-enaminone derivatives exhibit AIE properties. Interestingly, two types of crystals (**BrTE-G** and **BrTE-B**) of **BrTE** with different fluorescence properties were obtained. The crystal **BrTE-G** containing Br…π intermolecular interactions exhibits a nearly sevenfold higher fluorescence quantum yield (9.6%) compared to **BrTE-B**, the crystal without halogen bonding. Additionally, increasing the number of Br substituents leads to an even higher fluorescence quantum yield of **Br3TE** of up to 12.5%, whereas the fluorescence quantum yield of **TE** is only 2.1%.

Results and Discussion

The preparation procedures of TE, **BrTE**, and **Br3TE** are summarized in Scheme 1. The alkynol intermediate was facilely synthesized via a Grignard reaction between ethynylmagnesium bromide and benzaldehyde in dry tetrahydrofuran (THF) at room temperature, and then oxidized by 2-iodobenzoic acid (IBX) in ethyl acetate at 90 °C to obtain alkynone. An aza-Michael addition between alkynone and a secondary amine in methanol at room temperature produced **TE**, **BrTE**, and **Br3TE** in satisfactory yields.[18] Their chemical structures were fully characterized by ^{1}H and ^{13}C NMR spectroscopy, FT-IR, mass spectrometry, and elemental

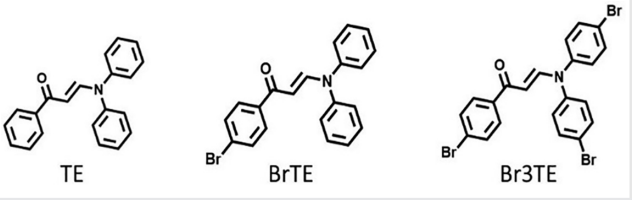

Figure 1 Structures of three *trans*-enaminone derivatives TE, **BrTE**, and **Br3TE**.

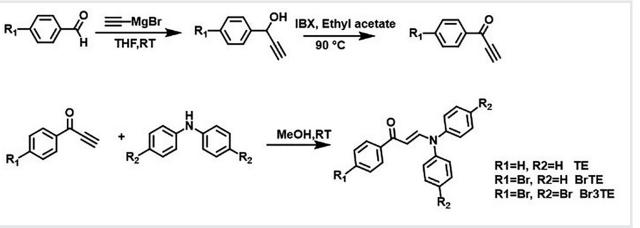

Scheme 1 Synthetic routes of three *trans*-enaminone derivatives TE, **BrTE**, and **Br3TE**.

analysis. The *trans*-conformations of the enaminone derivatives were confirmed by ^{1}H NMR spectra where the doublet at 6.03 ppm with a coupling constant of 12.8 Hz (Figures S12-S14) corresponds to the vinyl proton adjacent to the α-keto. All the compounds have good solubility in common organic solvents such as *n*-hexane (Hex), chloroform ($CHCl_3$), THF, and dimethylformamide (DMF). In $CHCl_3$ solution, **TE** shows an absorption maximum at 366 nm, while the absorption maxima of **BrTE** and **Br3TE** slightly red-shift to 370 and 369 nm, respectively (Figure S1 and Table S1). The three compounds show weak emission peaks at around 516 nm in $CHCl_3$. All of their emission spectra are sensitive to solvent polarity, and the emission peaks show bathochromic shifts of more than 60 nm with the increase in solvent polarity, indicating the existence of effective intramolecular charge transfer (Figure S2 and Table S1).

In order to study the luminescence of aggregates, typical AIE experiments were performed in DMF/H_2O mixtures with different water fractions (f_w). As shown in Figure 2, the emission of **BrTE** in DMF is rather weak. However, significantly enhanced emission is observed when the f_w exceeds 70%. Careful inspection of the photoluminescence spectra of **BrTE** reveals that the emission peak blue-shifts from 519 to 490 nm with the increase in f_w, which suggests the formation of aggregates with the restriction of the intramolecular charge transfer process.[19] Compared with pure DMF solution, the emission intensity of **BrTE** increases by about 28-fold in DMF/H_2O mixtures (f_w of 90%). Similar emission enhancements are also observed for **TE** and **Br3TE**

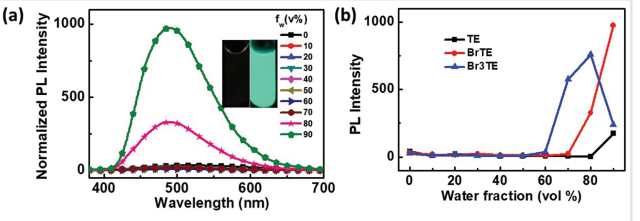

Figure 2 Photoluminescence (PL) spectra of **BrTE** (a) in the mixtures of DMF and water (10 μM, λ_{ex} = 360 nm, water contents 0–90%). Inset: photographs in DMF and DMF/H_2O (1:9) mixture under a 365-nm lamp. (b) Plots of PL intensity versus the composition of DMF/H_2O mixtures of TE, **BrTE**, and **Br3TE**.

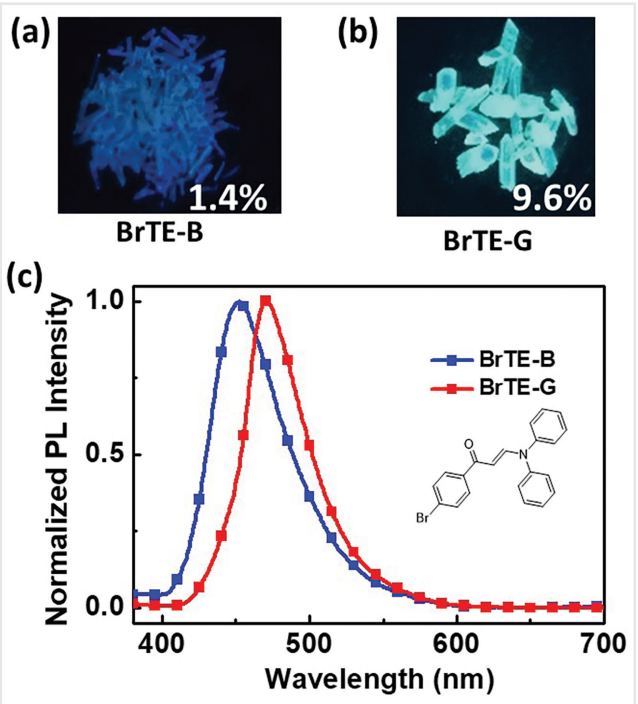

Figure 3 Photographic images of polymorphs **BrTE-B** (a) and **BrTE-G** (b); (c) fluorescence emission spectra of **BrTE-B** and **BrTE-G** (λ_{ex} = 360 nm).

(Figures 1b and S3). Clearly, the three *trans*-enaminone molecules possess AIE properties.

To gain further insight into the influence of bromine atoms on solid-state luminescence, the crystals of all three compounds were cultivated by slow vaporization of the corresponding compound solutions. To our surprise, two distinct types of **BrTE** crystals are obtained, the needle-like crystals with very weak deep-blue emission (**BrTE-B**) are obtained from methanol solution (Figure 3a) and the rod-like crystals with bright sky-blue emission (**BrTE-G**) from hexane solutions (Figure 3b). By the investigation of their photoluminescence (PL) spectra as shown in Figure 3c, the emission of **BrTE-B** shows a peak at 452 nm with a full-width at half-maximum (FWHM) of 59 nm, while **BrTE-G** exhibits red-shifted emission with a peak at 470 nm and a smaller FWHM of 47 nm, suggesting that the two crystals may have different molecular packing structures. Unfortunately, only polycrystals of **TE** and **Br3TE** rather than single crystals were obtained (Figure S5). The emission peaks of **TE** and **Br3TE** in crystals are found at 466 nm and 460 nm, respectively. The fluorescence emissions of all these crystals are confirmed by their luminescence lifetimes in nanoseconds (Table 1, Figure S7) and red-shifted phosphorescence emissions at low temperature (Figures S8 and S9). It is worth noting that the absolute fluorescence quantum yield of **BrTE-G** (9.6%) is nearly sevenfold than that of **BrTE-B** (1.4%). The fluorescence quantum yield of the crystal of **TE** is 2.1%, which is comparable to that of **BrTE-B** but much lower than that of **BrTE-G**. However, the crystal of **Br3TE** has the highest fluorescence quantum yield of 12.5% among the four crystals. Unlike the conventional heavy-atom quenching fluorescence, the introduction of bromine atoms into *trans*-enaminone derivatives could enhance fluorescence quantum yields in solid states.

The single-crystal X-ray diffraction data of **BrTE-B** and **BrTE-G** were further analyzed. As shown in Figure 4, **BrTE-B** and **BrTE-G** adopt similar distorted conformations, in which the benzene ring B is almost perpendicular to the conjugated molecular backbone. For **BrTE-B**, the distortion angle of the conjugated backbone C(O)–C = C–N is 177.80°. The dihedral angles between the conjugated backbone and the benzene rings A and C are 24.27° and 37.47°, respectively. However, **BrTE-G** adopts a relatively planar conformation since the conjugated backbone C(O)–C = C–N is nearly planar with a distortion angle of 179.96° and the dihedral angles between the conjugated backbone C(O)–C = C–N and the benzene rings A and C are 7.13° and 9.05° , respectively, which are much smaller than those in **BrTE-B**. A less twisted molecular conformation of **BrTE-G** could lead to the red-shifted emission. Both of **BrTE-B** and **BrTE-G** dimers assume antiparallel stacking between two bromine-substituted benzene rings with a π…π distance of 3.29 and 3.51 Å, respectively. In the **BrTE-G** dimer, Br…π interaction between the two adjacent molecules with a distance of 3.36 Å is formed, which allows the adjacent two molecules to lock together more tightly. Besides the Br…π and π…π interactions, more short intermolecular interactions of the crystal **BrTE-G**, including C–H…O (2.64, 2.52 Å), C–O…C (3.21 Å), and C–H…C (2.78, 2.77 Å) (Figure 5b), will enable the molecules to immobilize in a more rigidified environment. In contrast, in the crystal

Table 1 Summary of photophysical properties of TE, BrTE-B, BrTE-G, and Br3TE in crystal states at 298 K

Compound	λ_{em} (nm)	τ (ns)	Φ_F	k_r (10^8 s^{-1})	k_{nr} (10^8 s^{-1})
TE	466	0.73	2.1%	0.28	13.4
BrTE-B	452	0.67	1.4%	0.21	14.7
BrTE-G	470	1.09	9.6%	0.88	8.29
Br3TE	460	0.91	12.5%	1.37	9.62

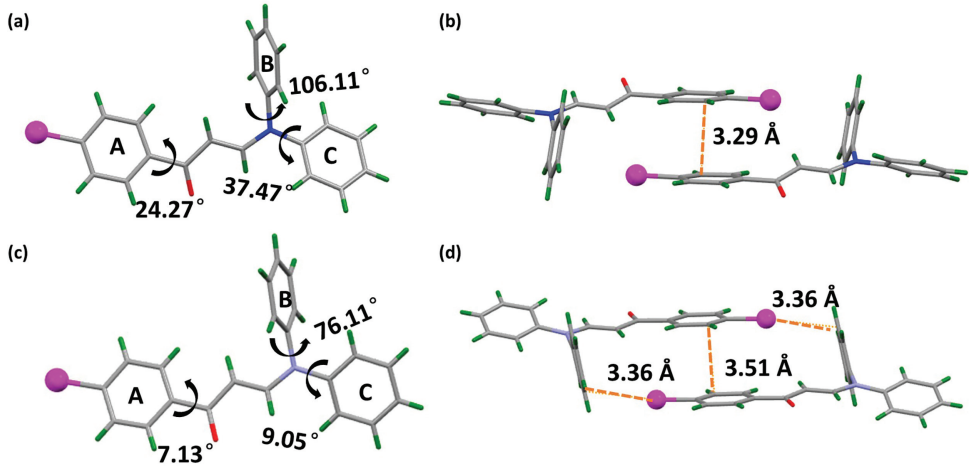

Figure 4 Molecular structure and dimer modes of **BrTE-B** (a, b) and **BrTE-G** (c, d).

BrTE-B, the less intermolecular interactions [C–H…π (2.86, 2.89 Å) and an additional π…π (3.33 Å)] reveal the loose molecular packing (Figure 5a). The smaller single-molecular average volume in the crystal lattice (419.7 $Å^3$) and the larger crystal density (1.497 g cm^{-3}) of **BrTE-G** compared to those of **BrTE-B** (426.9 $Å^3$ and 1.471 g cm^{-3}) also indicate that **BrTE-G** adopts a tighter molecular packing mode. According to thermogravimetric analysis (TGA) and differential scanning calorimetry (DSC) curves (Figure S6), both decomposition and melting temperatures of **BrTE-G** are higher than those of **BrTE-B**, which is well consistent with the more stable crystal structure and stronger intermolecular interactions of **BrTE-G**. As compared with the crystal **BrTE-B**, the tighter molecular stacking and more rigidified environment of the crystal **BrTE-G** suppress the molecular motions more efficiently, leading to significantly enhanced fluorescence quantum yields.

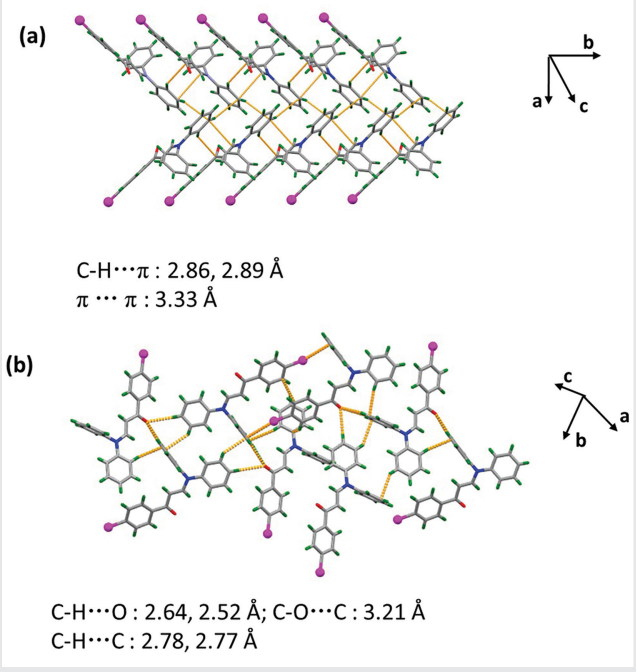

Figure 5 Molecular packing in **BrTE-B** (a) and **BrTE-G** (b), as viewed perpendicular to the direction in which the dimer is formed.

To further reveal the origin of fluorescence enhancement, the radiative (k_r) and nonradiative decay rates (k_{nr}) are estimated by combining the quantum yield [$\Phi_F = k_r/(k_r + k_{nr})$] and fluorescence lifetime results [$\tau = (k_r + k_{nr})^{-1}$]. As shown in Table 1, **BrTE-B** and **TE** show similar k_r and k_{nr}. For both of them, rather low k_r values and over high k_{nr} values lead to similar fluorescence quantum yields of around 2% because of their loose molecular stacking. Compared with **BrTE-B**, the k_r value of **BrTE-G** increases by about fourfold (from 0.21×10^8 to 0.88×10^8 s^{-1}) and the k_{nr} value nearly reduces to half (from 14.7×10^8 to 8.29×10^8 s^{-1}), which results in the high fluorescence quantum yield of 9.6%, indicating that more compact and rigidified crystal structures induced by Br…π halogen bonding and other strong molecular interactions may promote radiative transition but block the nonradiative relaxation efficiently. Compared with **BrTE-G**, a further increase in the k_r value of the **Br3TE** crystal leads to a higher fluorescence quantum yield of 12.5%, possibly due to more halogen bonding interactions. Therefore, the solid fluorescence of *trans*-enaminone can be regulated by adjusting the number of bromine atoms.

Theoretical calculations were carried out on the monomer and dimer derived from the single-crystal structures of **BrTE-B** and **BrTE-G** by TD-DFT at the level of the B3LYP/6-31G (d,p) basis set (Figure 6). For both **BrTE-G** and **BrTE-B**, the HOMOs are primarily localized on the electron-donating diphenylamine groups and enaminone [C(O)–C = C–N] moieties, and the LUMOs are delocalized on the whole conjugated skeletons, suggesting the existence of

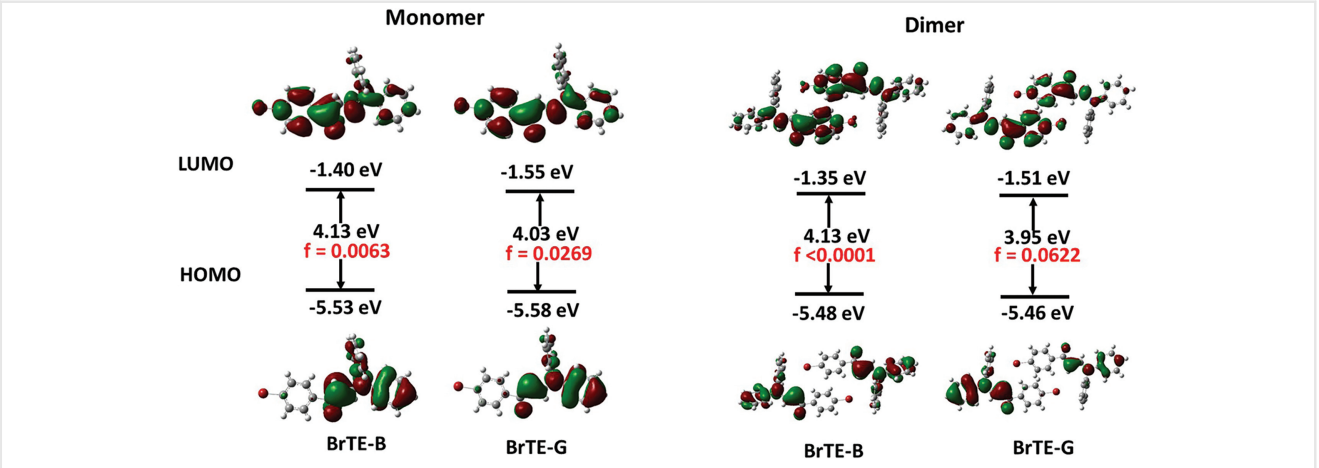

Figure 6 The frontier orbitals and energy levels of the monomers and dimers of **BrTE-B** and **BrTE-G** calculated by TD-DFT calculations at the B3LYP/6-31g (d,p) level.

intramolecular charge transfer. Both the monomers and dimers of **BrTE-G** exhibit a narrower calculated band gap and a larger oscillator strength than those of **BrTE-B**, which is in agreement with the red-shifted emission and higher k_r value of the **BrTE-G** crystal. Note that from the monomer to the dimer, the oscillator strength (f) of **BrTE-G** ($f = 0.0269$) further increases to 0.0622, while that of **BrTE-B** ($f = 0.0063$) almost decreases to zero, indicating that the formation of halogen bonding may help to achieve the higher radiative decay rate in crystal states.

We further studied the aggregated state of **BrTE-G** and **BrTE-B** using a quantum mechanics and molecular mechanics (QM/MM) approach,[20] and measured the dihedral angles of **BrTE-G** and **BrTE-B** in S_1 and S_0 states optimized in the crystal phase (Figures S10 and S11, and Table 2). From the S_0 state to the S_1 state, the bromine-substituted benzene ring against the enaminone moiety in the **BrTE-B** crystal undergoes a rotational motion with a relatively large dihedral angle change ($\Delta|S_1-S_0| = 14.09°$). In contrast, all the dihedral angle changes in the **BrTE-G** crystal are smaller than 5°. The smaller geometrical modification from the S_0 to S_1 state for the **BrTE-G** crystal reveals that the molecular conformation of **BrTE** is restricted in a more rigidified environment by halogen bonding and other intermolecular short contacts, which may account for its lower nonradiative decay rate and much stronger solid-state fluorescence as compared with **BrTE-B**.

Conclusions

In summary, we have synthesized three AIE-active *trans*-enaminone derivatives with and without bromine substituents (**TE**, **BrTE**, and **Br3TE**). Two single crystals (**BrTE-B** and **BrTE-G**) of **BrTE** with different fluorescence properties have been obtained. Notably, **BrTE-G** with Br…π halogen bonding exhibits nearly sevenfold and fivefold higher fluorescence quantum yields compared with **BrTE-B** and **TE**, respectively. The tighter molecular stacking and more rigidified environment caused by the intermolecular Br…π halogen bonding as well as the multiple stronger intermolecular contacts for the **BrTE-G** crystal can restrict molecular motions and promote the fluorescence emission process,

Table 2 Selected dihedral angles in their optimized geometric structures for BrTE-B and BrTE-G calculated in their crystal phase

	BrTE-B			BrTE-G		
	S_0	S_1	$\Delta\|S_1-S_0\|$	S_0	S_1	$\Delta\|S_1-S_0\|$
$C_1-C_6-C_7-C_8$	19.41°	5.32°	14.09°	2.25°	3.40°	1.15°
$C_7-C_8=C_9-N_1$	178.97°	−174.42°	5.31°	178.92°	178.72°	0.20°
$C_9-N_1-C_{10}-C_{15}$	−34.83°	−35.25°	1.46°	19.23°	14.64°	4.59°
$C_9-N_1-C_{16}=C_{17}$	98.88°	101.65°	2.77°	104.02°	106.03°	2.01°

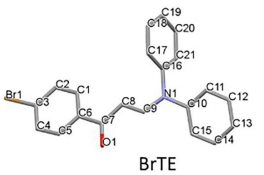

which is responsible for its high fluorescence quantum yield. Moreover, theoretical calculation also demonstrates that the formation of halogen bonding can result in a higher oscillator strength (f) and a smaller geometrical modification in the excited state, which may not only increase the probability of singlet radiative transition but also reduce the nonradiative decay rate, resulting in fluorescence enhancement in the solid states. Additionally, **Br3TE** with three bromine substituents exhibits an even higher fluorescence quantum yield than **BrTE-G**, indicating that the increased bromine atoms may be favorable for the formation of halogen bonding and fluorescence emission. We believe that manipulation of halogen bonding is a powerful strategy for designing bright fluorescent molecules in the solid state.

Experimental Section

Measurements and Characterization

The ^{1}H NMR spectra were recorded at 400 MHz (Bruker AV) or 500 MHz (Bruker AV) and the ^{13}C NMR spectra were recorded at 100 or 125 MHz with TMS as the internal standard. All shifts are given in ppm. All coupling constants (J values) are reported in hertz (Hz). High-resolution mass spectra were obtained by using LTQ Orbitrap Velos Pro. The elemental analysis was performed on a Bio-Rad elemental analysis system. Fourier-transform infrared spectra were obtained on a FT-IR Bruker Vertex 70 spectrometer. The power samples were prepared by adding model compounds and polymers into KBr, and the mixture was ground to a fine powder and pressed to form a disk. UV/Vis absorption spectra were recorded using a Perkin–Elmer Lambda 35 UV/Vis spectrometer, with a scan rate of 480 nm/min. Photoluminescence (PL) measurements were conducted utilizing a Hitachi F-7000 spectrophotometer equipped with a 150-W xenon lamp as the excitation source. The PLQYs were measured on an integrating sphere (Hamamatsu Photonics C9920-2). The empty and clean quartz cells (diameter is 15 mm, height is 5 mm) were set as the reference sample, and then the solid samples were encapsulated in quartz cells placed in the integral sphere. Each sample was tested three times, and the error was less than 1%. Fluorescence lifetimes were measured with an Edinburgh fluorescence spectrometer (FLSP-980). The lifetime (τ) of the luminescence was obtained by fitting the decay curve with a multiexponential decay function of

$$I(t) = \sum A_i \, e^{-t/\tau i}$$

where A_i and τ_i represent the amplitudes and lifetimes of the individual components for multiexponential decay profiles, respectively. The mean lifetime is $<\tau> = \Sigma A_i \tau_i$.

Crystal cultivation: **BrTE-B** and **BrTE-G** were cultivated from pure methanol (1 mg mL^{-1}) and hexane (1 mg mL^{-1}) solutions by slow evaporation at 25 °C for 1 week, respectively. The single-crystal X-ray diffraction experiments were carried out using a Bruker Smart APEX diffractometer with a CCD detector and graphite monochromator, Mo Kα radiation (λ = 0.71073 Å). The intensity data were recorded with the ω scan mode. Lorentz polarization factors were made for the intensity data and absorption corrections were performed using the SADABS program. The crystal structure was determined using the SHELXTL program and refined using full matrix least squares. All non-hydrogen atoms were assigned with anisotropic displacement parameters, whereas hydrogen atoms were placed at calculated positions theoretically and included in the final cycles of refinement in a riding model along with the attached carbons.

All calculations were performed with the Gaussian 09 program. The frontier orbitals and energy levels of **BrTE-G** and **BrTE-B** in the monomer molecule and dimer are calculated by TD-DFT calculations at the B3LYP/6-31g (d,p) level. The geometry structures for S0 and S1 in the crystalline phase were optimized by using DFT calculations and TD-DFT calculations at the ONIOM (B3LYP/6-31G (d,p): UFF) level.

Materials

All chemicals and reagents were used as received from commercial sources without further purification. Solvents for chemical synthesis were purified according to the standard procedures.

1-Phenylprop-2-yn-1-ol: a solution of ethynylmagnesium bromide (0.5 M in THF, 26 mL, 13 mmol, 1.3 equiv.) was added at 0 °C to a solution of the corresponding benzaldehyde (10 mmol) in THF (20 mL). After the mixture had been stirred for 2 h at room temperature, a saturated solution of NH_4Cl (20 mL) was added to the solution and the THF was evaporated under vacuum. The aqueous phase was extracted three times with ethyl acetate and the organic layers were washed with water and brine and then dried with anhydrous Na_2SO_4. After evaporation of the solvent, the resulting crude product was purified by column chromatography (heptane/ethyl acetate = 20/1, v/v) to give as yellow solid (1.0 g, 7.9 mmol, 79%). ^{1}H NMR (400 MHz, $CDCl_3$): δ (ppm) 7.55 (m, 2 H, Ar–H), 7.36 (m, 3 H, Ar–H), 5.48 (d, J = 2.2 Hz, 1 H, CH), 2.68 (d, J = 2.2 Hz, 1 H, C≡CH), 2.05 (s, 1 H, OH); ^{13}C NMR (100 MHz, $CDCl_3$): δ (ppm) 140.2, 128.7, 128.6, 126.7 (C_{Ar}), 83.5, 74.8 (C≡C), 64.4 (CH).

1-Phenylprop-2-yn-1-one: IBX (2.8 g, 10 mmol, 2 equiv.) was added in one portion to a solution of

1-phenylprop-2-yn-1-ol (660 mg, 5 mmol, 1 equiv.) in ethyl acetate (25 mL). The mixture was heated at 90 °C and stirred overnight. After cooling to room temperature, the mixture was filtered and ethyl acetate was evaporated under vacuum. The resulting crude product was purified by column chromatography (heptane/ethyl acetate = 100/1, v/v) to give in pure form as a yellow solid (611 mg, 4.7 mmol, 94%). ^{1}H NMR (400 MHz, $CDCl_3$) δ (ppm) 8.1 (m, 2 H, Ar–H), 7.65 (m, 1 H, Ar–H), 7.51 (m, 2 H, Ar–H), 3.44 (s, 1 H, C≡CH). ^{13}C NMR (100 MHz, $CDCl_3$): δ (ppm) 177.7 (C = O), 136.2, 134.5, 129.7, 128.7 (C_{Ar}), 80.7, 80.3 (C≡C).

(*E*)-3-(Diphenylamino)-1-phenylprop-2-en-1-one (TE): diphenylamine (1.01g, 6 mmol) was added in a methanol solution of 1-phenylprop-2-yn-1-one (0.65 g, 5 mmol) and the reaction mixture was stirred overnight at room temperature. The solution was then concentrated by rotary evaporation and purified by silica gel column chromatography (petroleum ether/ethyl acetate = 10/1, v/v) to give TE as a white solid (1.09 g, 4.4 mmol, 73%). m.p. 118–120 °C; ^{1}H NMR (500 MHz, $CDCl_3$): δ (ppm) 8.46 (d, J = 12.8 Hz, 1 H, C = CH), 7.78 (d, J = 8.5 Hz, 2 H, Ar–H), 7.41 (m, 7 H, Ar–H), 7.27 (d, J = 7.6 Hz, 2 H, Ar–H), 7.19 (d, J = 7.6 Hz, 4 H, Ar–H), 6.03 (d, J = 12.8 Hz, 1 H, CH = C); ^{13}C NMR (125 MHz, $CDCl_3$): δ (ppm) 189.6 (C = O), 148.9 (C = C), 139.5, 131.6, 129.8, 128.2, 127.8 (C_{Ar}), 100.4 (C = C); IR (KBr, cm^{-1}) 3050, 1645, 1531, 1490, 1242, 1048, 700; HRMS (EI) calcd: m/z = 299.1310, found: m/z = 300.1386 $[M + H]^+$; anal. calcd for C21H17NO: C 84.25, H 5.72, N 4.68, found: C 83.71, H 4.61, N 4.61.

1-(4-Bromophenyl)prop-2-yn-1-ol: a solution of ethynylmagnesium bromide (0.5 M in THF, 195 mL, 97.5 mmol, 1.3 equiv.) was added at 0 °C to a solution of the corresponding 4-bromobenzaldehyde (13.9 g, 75 mmol) in THF (20 mL). After the mixture had been stirred for 2 h at room temperature, a saturated solution of NH_4Cl (100 mL) was added to the solution and the THF was evaporated under vacuum. The aqueous phase was extracted three times with ethyl acetate and the organic layers were washed with water and brine and then dried with anhydrous Na_2SO_4. After evaporation of the solvent, the resulting crude product was purified by column chromatography (heptane/ethyl acetate = 20/1, v/v) to give in pure form a yellow solid (12.5 g, 59 mmol, 79%). ^{1}H NMR (400 MHz, $CDCl_3$): δ (ppm) 7.52 (d, J = 8.5 Hz, 2 H, Ar–H), 7.43 (d, J = 8.5 Hz, 2H, Ar–H), 5.43 (d, J = 2.2 Hz,1 H, CH), 2.68 (d, J = 2.2 Hz, 1 H, C≡CH) , 2.08 (s, 1 H, OH). ^{13}C NMR (100 MHz, $CDCl_3$): δ (ppm) 139.0, 131.9, 128.3 (C_{Ar}), 82.9, 75.2 (C≡C), 63.8 (CH).

1-(4-Bromophenyl)prop-2-yn-1-one: IBX (30.7 g, 110 mmol, 2 equiv.) was added in one portion to a solution of 1-(4-bromophenyl)prop-2-yn-1-ol (11.8 g, 55 mmol) in ethyl acetate (25 mL). The mixture was heated at 90 °C and stirred overnight. After recooling to room temperature, the mixture was filtered and ethyl acetate was evaporated under vacuum. The resulting crude product was purified by column chromatography (heptane/ethyl acetate 100/1, v/v) to give in pure form as a yellow solid (10.7 g, 51 mmol, 92%). ^{1}H NMR (400 MHz, $CDCl_3$): δ (ppm) 8.02 (d, J = 8.7 Hz, 2 H, Ar–H), 7.64 (d, J = 8.7 Hz, 2 H, Ar–H), 3.46 (s, 1 H, C≡CH). ^{13}C NMR (100 MHz, $CDCl_3$): δ (ppm) 176.5 (C = O), 135.1, 131.6, 131.3, 130.1 (C_{Ar}), 81.3, 79.8 (C≡C).

(*E*)-1-(4-Bromophenyl)-3-(diphenylamino)prop-2-en-1-one (BrTE): diphenylamine (2.03 g, 12 mmol) was added in a methanol solution of 1-(4-bromophenyl) prop-2-yn-1-one (2.09 g, 10 mmol), and the reaction mixture was stirred overnight at room temperature. The solution was then concentrated by rotary evaporation and purified by silica gel column chromatography (petroleum ether/ethyl acetate = 20/1, v/v) to give **BrTE** as a white solid (2.94, 7.8 mmol, 78%). M.p. 150–152 °C; ^{1}H NMR (500 MHz, $CDCl_3$): δ (ppm) 8.50 (d, J = 12.5 Hz, 1 H, C = CH), 7.64 (d, J = 8.5 Hz, 2 H, Ar–H), 7.50 (d, J = 8.5 Hz, 2 H, Ar–H), 7.43 (t, J = 7.2 Hz, 4 H, Ar–H), 7.30 (m, 2 H, Ar–H), 7.19 (d, J = 7.2 Hz, 4 H, Ar–H), 5.96 (d, J = 12.5 Hz, 1 H, CH = C); ^{13}C NMR (125 MHz, $CDCl_3$): δ (ppm) 188.3 (C = O), 149.6 (C = C), 138.1, 131.5, 129.9, 129.4, 126.6 (C_{Ar}), 99.7 (C = C); IR (KBr) 3061, 1648, 1538, 1486, 1248, 1052, 705 cm^{-1}; HRMS (EI) calcd: m/z = 377.0415, found: m/z = 378.0482 $[M + H]^+$; anal. calcd for $C_{21}H_{16}BrNO$: C 66.52, H 4.29, N 3.63, found: C 66.68, H 4.26, N 3.70.

(E)-3-(Bis(4-bromophenyl)amino)-1-(4-bromophenyl) prop-2-en-1-one (Br3TE): bis(4-bromophenyl)amine (1.96, 6 mmol) was added in a methanol solution of 1-(4-bromophenyl)prop-2-yn-1-one (1.05 g, 5 mmol), and the reaction mixture was stirred overnight at room temperature. The solution was then concentrated by rotary evaporation and purified by silica gel column chromatography (petroleum ether/ethyl acetate = 20/1, v/v) to give **Br3TE** as a white solid (1.55 g, 2.9 mmol, 58%). M.p. 186–188 °C; ^{1}H NMR (500 MHz, $CDCl_3$): δ (ppm) 8.30 (d, J = 12.8 Hz, 1 H, C = CH), 7.65 (d, J = 8.5 Hz, 2 H, Ar–H), 7.60–7.49 (m, 6 H, Ar–H), 7.04 (d, J = 8.5 Hz, 4 H, Ar–H), 6.00 (d, J = 12.8 Hz, 1 H, CH = C); ^{13}C NMR (125 MHz, $CDCl_3$): δ (ppm) 188.3 (C = O), 148.1 (C = C), 137.9, 133.4, 131.6, 129.3, 126.9 (C_{Ar}), 100.9 (C = C); IR (KBr) 3048, 1641, 1542, 1487, 1251, 804 cm^{-1}; HRMS (EI) calcd: m/z = 534.8626, found: m/z = 535.8677 $[M + H]^+$; anal. calcd for C21H14Br3NO: C 66.52, H 4.29, N 3.63, found: C 66.68, H 4.26, N 3.70.

Funding Information

This work was financially supported by the Strategic Priority Research Program of the Chinese Academy of Sciences (Grant No. XDB12010200) and the National Natural Science

Foundation of China (Grant Nos. 51833009, 21674111, 21574131, 51973211, and 21322403).

Supporting Information

Supporting information for this article is available online at https://doi.org/10.1055/s-0040-1701249.

References

(1) (a) Chen, C.-T. *Chem. Mater.* **2004**, *16*, 4389. (b) Ding, D.; Li, K.; Liu, B.; Tang, B. Z. *Acc. Chem. Res.* **2013**, *46*, 2441. (c) Luo, D.; Xiao, P.; Liu, B. *Chem. Rec.* **2019**, *19*, 1596. (d) Sedgwick, A. C.; Wu, L.; Han, H. H.; Bull, S. D.; He, X. P.; James, T. D.; Sessler, J. L.; Tang, B. Z.; Tian, H.; Yoon, J. *Chem. Soc. Rev.* **2018**, *47*, 8842.

(2) (a) Li, Q.; Li, Z. *Adv. Sci.* **2017**, *4*, 1600484. (b) Mei, J.; Leung, N. L.; Kwok, R. T.; Lam, J. W.; Tang, B. Z. *Chem. Rev.* **2015**, *115*, 11718. (c) Naito, H.; Morisaki, Y.; Chujo, Y. *Angew. Chem. Int. Ed.* **2015**, *54*, 5084.

(3) Luo, J.; Xie, Z.; Lam, J. W.; Cheng, L.; Chen, H.; Qiu, C.; Kwok, H. S.; Zhan, X.; Liu, Y.; Zhu, D.; Tang, B. Z. *Chem. Commun.* **2001**, 1740.

(4) (a) Yuan, W. Z.; Tan, Y.; Gong, Y.; Lu, P.; Lam, J. W.; Shen, X. Y.; Feng, C.; Sung, H. H.; Lu, Y.; Williams, I. D.; Sun, J. Z.; Zhang, Y.; Tang, B. Z. *Adv. Mater.* **2013**, *25*, 2837. (b) Cai, S.; Shi, H.; Tian, D.; Ma, H.; Cheng, Z.; Wu, Q.; Gu, M.; Huang, L.; An, Z.; Peng, Q.; Huang, W. *Adv. Funct. Mater.* **2018**, *28*, 1705045.

(5) (a) Yu, T.; Ou, D.; Yang, Z.; Huang, Q.; Mao, Z.; Chen, J.; Zhang, Y.; Liu, S.; Xu, J.; Bryce, M. R.; Chi, Z. *Chem. Sci.* **2017**, *8*, 1163. (b) Xia, G.; Jiang, Z.; Shen, S.; Liang, K.; Shao, Q.; Cong, Z.; Wang, H. *Adv. Opt. Mater.* **2019**, *7*, 1801549.

(6) Sagara, Y.; Kato, T. *Angew. Chem. Int. Ed.* **2008**, *47*, 5175.

(7) Song, X.; Zhang, Z.; Zhang, S.; Wei, J.; Ye, K.; Liu, Y.; Marder, T. B.; Wang, Y. *J. Phys. Chem. Lett.* **2017**, *8*, 3711.

(8) (a) Xu, B.; Li, W.; He, J.; Wu, S.; Zhu, Q.; Yang, Z.; Wu, Y. C.; Zhang, Y.; Jin, C.; Lu, P. Y.; Chi, Z.; Liu, S.; Xu, J.; Bryce, M. R. *Chem. Sci.* **2016**, *7*, 5307. (b) He, Z.; Zhang, L.; Mei, J.; Zhang, T.; Lam, J. W. Y.; Shuai, Z.; Dong, Y. Q.; Tang, B. Z. *Chem. Mater.* **2015**, *27*, 6601. (c) Wu, Q.; Ma, H.; Ling, K.; Gan, N.; Cheng, Z.; Gu, L.; Cai, S.; An, Z.; Shi, H.; Huang, W. *ACS Appl. Mater. Interfaces* **2018**, *10*, 33730. (d) Zhang, Y.; Feng, Y.-Q.; Tian, X.-X.; Wang, J.-H.; Li, H.; Han, G.; Li, D. *Adv. Opt. Mater.* **2018**, *6*, 1800903.

(9) (a) Desiraju, G. R.; Ho, P. S.; Kloo, L.; Legon, A. C.; Marquardt, R.; Metrangolo, P.; Politzer, P.; Resnati, G.; Rissanen, K. *Pure. Appl. Chem.* **2013**, *85*, 1711. (b) Cavallo, G.; Metrangolo, P.; Milani, R.; Pilati, T.; Priimagi, A.; Resnati, G.; Terraneo, G. *Chem. Rev.* **2016**, *116*, 2478.

(10) Wang, C.; Danovich, D.; Mo, Y.; Shaik, S. *J. Chem. Theory Comput.* **2014**, *10*, 3726.

(11) (a) Christopherson, J. C.; Topić, F.; Barrett, C. J.; Friščić, T. *Cryst. Growth Des.* **2018**, *18*, 1245. (b) Tepper, R.; Schubert, U. S. *Angew. Chem. Int. Ed.* **2018**, *57*, 6004.

(12) (a) Bunchuay, T.; Docker, A.; Martinez-Martinez, A. J.; Beer, P. D. *Angew. Chem. Int. Ed.* **2019**, *58*, 13823. (b) Gropp, C.; Husch, T.; Trapp, N.; Reiher, M.; Diederich, F. *J. Am. Chem. Soc.* **2017**, *139*, 12190. (c) Gropp, C.; Quigley, B. L.; Diederich, F. *J. Am. Chem. Soc.* **2018**, *140*, 2705.

(13) Bulfield, D.; Huber, S. M. *Chem. Eur. J.* **2016**, *22*, 14434.

(14) (a) Ang, S. J.; Chwee, T. S.; Wong, M. W. *J. Phys. Chem. C.* **2018**, *122*, 12441. (b) Wang, J.; Wang, C.; Gong, Y.; Liao, Q.; Han, M.; Jiang, T.; Dang, Q.; Li, Y.; Li, Q.; Li, Z. *Angew. Chem. Int. Ed.* **2018**, *57*, 16821. (c) Kanosue, K.; Ando, S. *ACS Macro Lett.* **2016**, *5*, 1301.

(15) (a) Kenry, Chen, C.; Liu, B. *Nat. Commun.* **2019**, *10*, 2111. (b) Lucenti, E.; Forni, A.; Botta, C.; Giannini, C.; Malpicci, D.; Marinotto, D.; Previtali, A.; Righetto, S.; Cariati, E. *Chem. Eur. J.* **2019**, *25*, 2452. (c) Wang, J.; Wang, C.; Gong, Y.; Liao, Q.; Han, M.; Jiang, T.; Dang, Q.; Li, Y.; Li, Q.; Li, Z. *Angew. Chem. Int. Ed.* **2018**, *57*, 16821. (d) Bolton, O.; Lee, K.; Kim, H. J.; Lin, K. Y.; Kim, J. *Nat. Chem.* **2011**, *3*, 205.

(16) (a) Chen, W.; Zhang, S.; Dai, G.; Chen, Y.; Li, M.; Zhao, X.; Chen, Y.; Chen, L. *Chem. Eur. J.* **2019**, *25*, 469. (b) D'Aléo, A.; Saul, A.; Attaccalite, C.; Fages, F. *Mater. Chem. Front.* **2019**, *3*, 86. (c) DeRosa, C. A.; Kerr, C.; Fan, Z.; Kolpaczynska, M.; Mathew, A. S.; Evans, R. E.; Zhang, G.; Fraser, C. L. *ACS Appl. Mater. Interfaces* **2015**, *7*, 23633. (d) Shi, H.; An, Z.; Li, P.-Z.; Yin, J.; Xing, G.; He, T.; Chen, H.; Wang, J.; Sun, H.; Huang, W.; Zhao, Y. *Cryst. Growth Des.* **2016**, *16*, 808. (e) Yan, D.; Delori, A.; Lloyd, G. O.; Friscic, T.; Day, G. M.; Jones, W.; Lu, J.; Wei, M.; Evans, D. G.; Duan, X. *Angew. Chem. Int. Ed.* **2011**, *50*, 12483. (f) Salunke, J. K.; Durandin, N. A.; Ruoko, T. P.; Candeias, N. R.; Vivo, P.; Vuorimaa-Laukkanen, E.; Laaksonen, T.; Priimagi, A. *Sci. Rep.* **2018**, *8*, 14431.

(17) Li, H.; Shu, H.; Liu, Y.; Wu, X.; Tian, H.; Tong, H.; Wang, L. *Adv. Opt. Mater.* **2019**, *7*, 1801719.

(18) (a) Chisholm, D. R.; Valentine, R.; Pohl, E.; Whiting, A. *J. Org. Chem.* **2016**, *81*, 7557. (b) Chassaing, S.; Kueny-Stotz, M.; Isorez, G.; Brouillard, R. *Eur. J. Org. Chem.* **2007**, *15*, 2438.

(19) (a) Sasaki, S.; Drummen, G. P. C.; Konishi, G.-I. *J. Mater. Chem. C* **2016**, *4*, 2731. (b) Zbigniew, R.; Grabowski, K. R. *Chem. Rev.* **2003**, *103*, 3899.

(20) Isayama, K.; Aizawa, N.; Kim, J. Y.; Yasuda, T. *Angew. Chem. Int. Ed.* **2018**, *57*, 11982.